

Modeling the direct current superconducting quantum interference device coupled to the multiturn input coil. II

K. Enpuku, R. Cantor, and H. Koch

Citation: [Journal of Applied Physics](#) **71**, 2338 (1992); doi: 10.1063/1.351353

View online: <http://dx.doi.org/10.1063/1.351353>

View Table of Contents: <http://scitation.aip.org/content/aip/journal/jap/71/5?ver=pdfcov>

Published by the [AIP Publishing](#)

Articles you may be interested in

[Superconducting multiturn flux transformers for radio frequency superconducting quantum interference devices](#)

J. Appl. Phys. **88**, 5966 (2000); 10.1063/1.1322382

[Effect of capacitive feedback on the characteristics of direct current superconducting quantum interference device coupled to a multiturn input coil](#)

J. Appl. Phys. **82**, 457 (1997); 10.1063/1.365838

[Automatic adjustment of bias current for direct current superconducting quantum interference device](#)

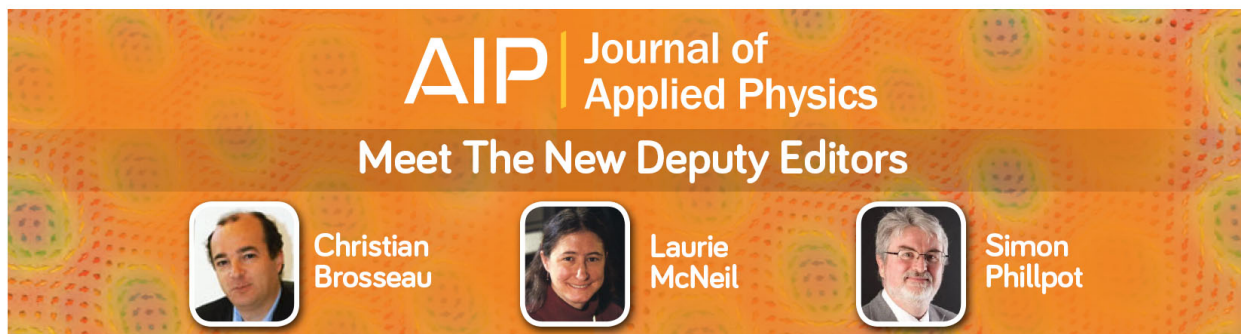
Rev. Sci. Instrum. **64**, 583 (1993); 10.1063/1.1144182

[Modeling the dc superconducting quantum interference device coupled to the multiturn input coil. III](#)

J. Appl. Phys. **72**, 1000 (1992); 10.1063/1.351824




[Modeling the dc superconducting quantum interference device coupled to the multiturn input coil](#)

J. Appl. Phys. **69**, 7295 (1991); 10.1063/1.347576



AIP | Journal of
Applied Physics

Meet The New Deputy Editors

	Christian Brosseau		Laurie McNeil		Simon Phillpot
---	-------------------------------	---	--------------------------	--	---------------------------

Modeling the direct current superconducting quantum interference device coupled to the multiturn input coil. II.

K. Enpuku,^{a)} R. Cantor, and H. Koch

Physikalisch-Technische Bundesanstalt, Abbestr. 10-12, W-1000 Berlin 10, Germany

(Received 17 October 1991; accepted for publication 15 November 1991)

A complete circuit model of a dc superconducting quantum interference device (SQUID) coupled to a multiturn input coil has been developed. With this model, it is shown that the rf properties of the coupled SQUID can be calculated using only the given parameters of the SQUID. There are no adjustable parameters. The resonant structures in the SQUID characteristics caused by the presence of the input coil have been quantitatively studied. Methods to suppress the resonant structures have also been investigated. It is shown that the present circuit model explains well the experimentally observed rf properties of coupled SQUIDs. The present circuit model is therefore useful for the design of highly sensitive SQUIDs.

I. INTRODUCTION

Direct current SQUIDs (superconducting quantum interference devices) operating at liquid-helium temperature have long been intensively studied. One of the problems in developing a highly sensitive SQUID is the effect of the multiturn input coil on the SQUID characteristics. It has been shown experimentally that the SQUID characteristics are degraded significantly when a multiturn input coil is coupled to the SQUID.¹⁻⁵ It has also been shown that damping resistors connected in parallel with the input coil or the SQUID washer are useful to prevent the degradation of the SQUID characteristics.³⁻⁷ There have been, however, only a few theoretical studies^{4,8-10} of the effect of the input coil, and the mechanism causing the degradation of the SQUID characteristics is not yet fully understood. It is very important to clarify the mechanism in order to develop highly sensitive SQUIDs.

In the previous theoretical studies,^{4,8} the effect of the input coil has been studied by taking into account the parasitic capacitance introduced by the input coil: The parasitic capacitance is represented by an additional capacitance in parallel with the input coil. It has been shown⁸ that the resonance caused by the parasitic capacitance and the inductance of the input coil considerably affects the SQUID characteristics, and that the suppression of this resonance is important to improve the SQUID performance. Although this model shows the importance of this resonance, the model is too simple for quantitative study; from the geometry of the input coil, we can expect many other resonances due to the formation of standing waves in the input coil. In order to quantitatively study the effect of the input coil, we need to develop a more complete model of the coupled SQUID.

In a previous paper⁹ (hereafter referred to as I), the rf properties of a SQUID were determined using an expanded model of the SQUID. Based on the observed rf properties, a circuit model of the coupled SQUID was proposed: The

input coil is represented by a set of resonant circuits, each of which couples to the SQUID via a mutual inductance. The previous circuit model, however, was not complete: The values of each element of the circuit model needed to be specified. In the previous papers,^{9,10} the values of each element were adjustable parameters which were determined by comparison with the experimental results. For SQUID design, however, a more complete circuit model is needed; i.e., a circuit model is needed from which the rf properties of the SQUID can be calculated using the known parameters of the SQUID.

In this paper, a complete circuit model of a dc SQUID with a closely coupled input coil is presented. Using this model, the rf properties of the SQUID have been quantitatively studied. The rf properties calculated from the present model are shown to explain well the experimental results without any adjustable parameters. Using the rf properties, the effects of the input coil on the SQUID characteristics are also discussed.

II. CIRCUIT MODEL

In Fig. 1, a schematic figure of the SQUID coupled to a multiturn input coil is shown. For the following calculations, we define several variables as shown in Fig. 1. The number of turns of the input coil is N , and we divide the coupling circuit into N sections. The shaded area of the input coil shown in Fig. 1 represents the m th section. The rf currents flowing in the input coil are defined by I_m ($m = 1, N + 1$) at the ends of each section, as shown in Fig. 1. The rf voltages in the input coil are defined by $V_{i,m}$ ($m = 1, N + 1$) at the ends of each section, which are denoted by the solid circles in Fig. 1. The voltages in the SQUID washer are defined by $V_{sb,m}$ ($m = 1, N$) and $V_{sa,m}$ ($m = 2, N + 1$), as denoted by the open circles in Fig. 1; the right- and left-hand sides of the SQUID washer slit are denoted by b and a , respectively. A current I_{sq} is fed to the SQUID washer using a rf current source, and the rf voltage V is measured across the terminals A and B.

In the following, we show the scheme used to calculate the rf currents and voltages in each section. In the calcu-

^{a)}On leave from the Department of Electronics, Kyushu University, Fukuoka 812, Japan.

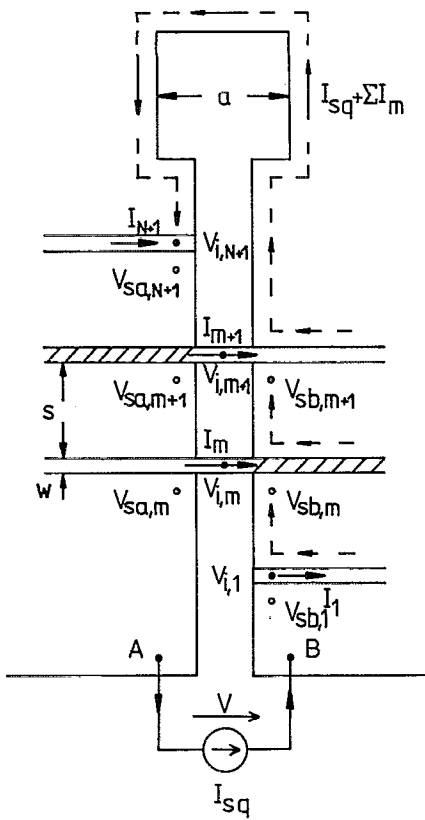


FIG. 1. Schematic figure of the SQUID coupled to the multiturn input coil. The input coil is divided into N sections, and the shaded region corresponds to the m th section. Several variables are defined at the ends of each section. The impedance seen from the terminals A and B of the SQUID washer is defined by $Z_{AB} = V/I_{sq}$.

lation, we assume that, in each section of the coupling circuit, the rf fields between the input coil and the SQUID washer propagate in the same way as in the case of a standard stripline¹¹. The input coil and the SQUID washer form a transmission line for the rf fields. This assumption has been partly confirmed by an experiment using an expanded model.^{9,10} In this case, each section of the coupling circuit can be represented by a transmission line, and the coupling circuit can be expressed by a set of transmission lines, as shown in Fig. 2. In Fig. 2, the voltages $V_{ta,m} = V_{i,m} - V_{sa,m}$ and $V_{tb,m} = V_{i,m} - V_{sb,m}$ represent the

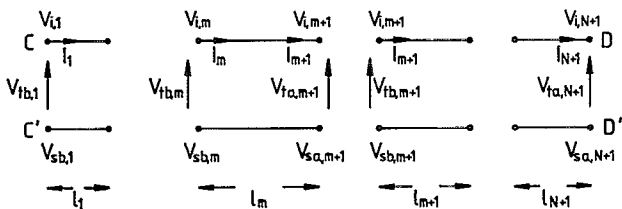


FIG. 2. Circuit model to study the rf properties of the coupling circuit between the SQUID washer and the input coil. The coupling circuit is represented by a set of transmission lines, each of which corresponds to the section defined in Fig. 1. The voltages $V_{ta,m} = V_{i,m} - V_{sa,m}$ and $V_{tb,m} = V_{i,m} - V_{sb,m}$ are the voltages across the transmission line at the end of each section.

voltages across the transmission line at the ends of each section. The length of each section is denoted by l_m , and the terminals of the input coil are denoted by C and D, as shown in Fig. 2.

We obtain the rf currents I_m and the voltages $V_{ta,m}$ and $V_{tb,m}$ in each transmission line shown in Fig. 2 as follows. Using the properties of the transmission line, a relation between the rf currents and the voltages at both ends of each transmission line can be written as

$$I_{m+1} = I_m \cos kl_m - j \frac{V_{tb,m}}{z_0} \sin kl_m \quad (1)$$

$$\frac{V_{ta,m+1}}{z_0} = -j I_m \sin kl_m + \frac{V_{tb,m}}{z_0} \cos kl_m \quad (2)$$

for $m = 1, \dots, N$, where z_0 is the characteristic impedance of the transmission line, $k = (\omega/v_c)(1 - j/2Q)$ is the complex wave number, ω is the angular frequency, v_c is the velocity of the electromagnetic waves, and Q is the quality factor of the transmission line. From Eqs. (1) and (2), we obtain the relation between the set $(I_{m+1}, V_{ta,m+1})$ and $(I_m, V_{tb,m})$ shown in Fig. 2.

Next, a relation between $V_{tb,m}$ and $V_{ta,m}$ is obtained as follows. When a rf current I_m flows in the input coil, an image current flows in the SQUID washer, as shown by the dashed lines in Fig. 1; the value of the image current is the same as I_m , but the direction is opposite. Due to the existence of the slit in the SQUID washer, the image current must flow along the slit, and pass the hole of the SQUID washer, as shown in Fig. 1. When the slit inductance is not zero, the image currents cause a voltage drop along the slit. If we take the voltage drop due to the slit inductance into account, we obtain the following relation between the voltages $V_{ta,m}$ and $V_{tb,m}$:

$$V_{tb,m} = V_{ta,m} - V + j\omega\Delta L_{s1} \left(m I_{sq} + \sum_{i=1}^{m-1} (m - i) I_i \right), \quad (3)$$

where $\Delta L_{s1} = L_{s1}/(N + 1)$ is the slit inductance between each section, and L_{s1} is the total slit inductance of the SQUID washer. Note that the third term on the right-hand side of Eq. (3) represents the voltage drop due to the slit inductance.

Substituting Eq. (3) into Eqs. (1) and (2), we obtain a relation between the set of $(I_m, V_{ta,m})$. It can be shown from Eqs. (1) and (2) that the variables I_m and $V_{ta,m}$ can be expressed as a linear function of I_1 , $V_{tb,1}$, V , and I_{sq} ; here, I_1 and $V_{tb,1}$ are the rf current and voltage, respectively, at the first section of the transmission line, as shown in Fig. 2 (at terminal C), and V and I_{sq} are the voltage and current, respectively, at the terminal of the SQUID washer, as shown in Fig. 1. Therefore, we can express I_m and $V_{ta,m}$ as

$$I_m = A_m I_1 + B_m \frac{V_{tb,1}}{z_0} + C_m \frac{V}{z_0} + D_m I_{sq}, \quad (4)$$

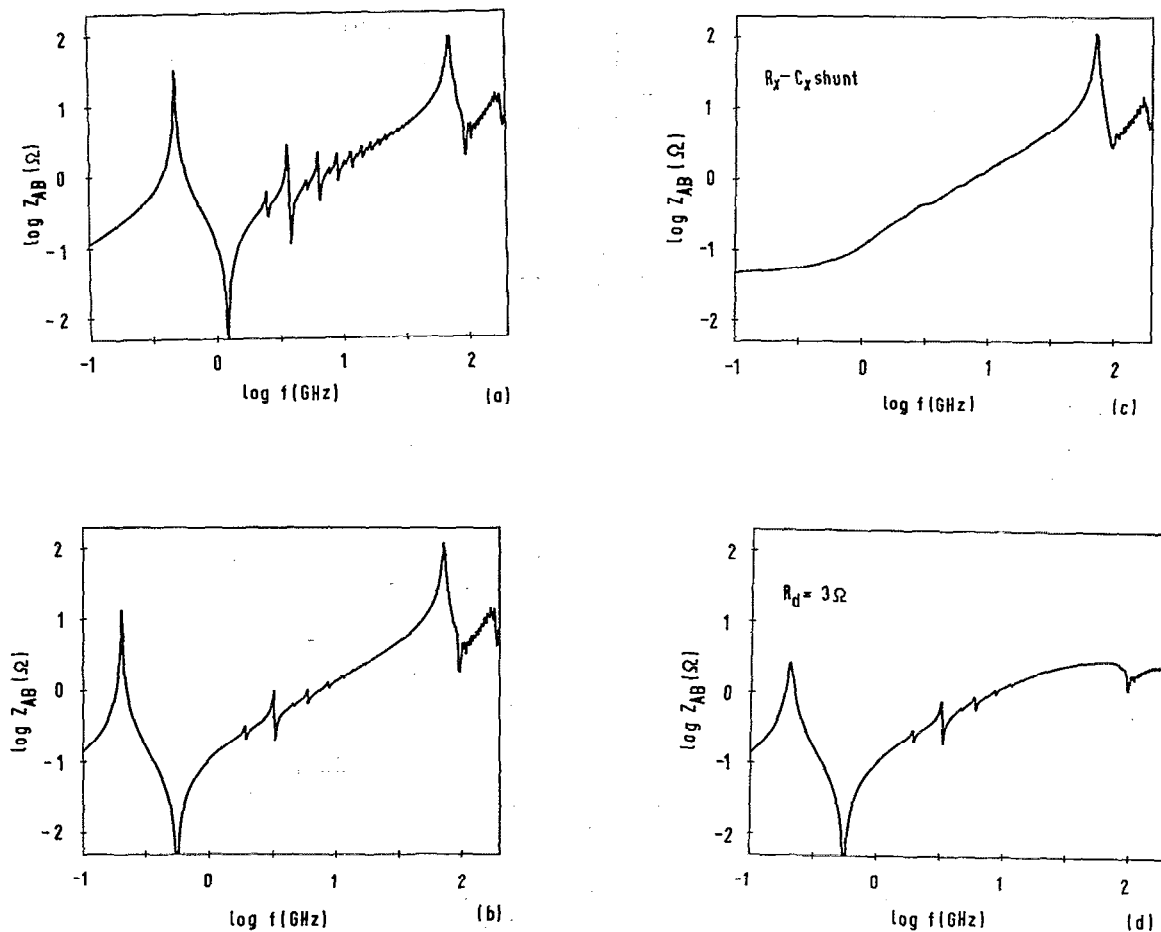


FIG. 3. The impedance Z_{AB} calculated for different cases. In each case, the absolute value of Z_{AB} is shown as a function of frequency, f : (a) conventional case, both terminals of the input coil are open; (b) one terminal of the input coil is shorted to the SQUID washer; (c) an $R_x - C_x$ shunt is connected between the input coil and the SQUID washer; and (d) a damping resistor $R_d = 3 \Omega$ is connected in parallel with the SQUID washer.

$$\frac{V_{ta,m}}{z_0} = E_m I_1 + F_m \frac{V_{tb,1}}{z_0} + G_m \frac{V}{z_0} + H_m I_{sq} \quad (5)$$

for $m = 2, \dots, N+1$. In Eqs. (4) and (5), $A_m - H_m$ are coefficients with complex values, and can be calculated if the parameters of the SQUID are given (see Appendix A).

The variables I_1 and $V_{tb,1}$ in Eqs. (4) and (5) can be determined from the boundary conditions of the input coil, and can be expressed as a linear function of V and I_{sq} (see Appendix B). Therefore, when the boundary conditions of the input coil are given, we can calculate from Eqs. (4) and (5) the rf current I_m and the voltage $V_{ta,m}$ in each section of the coupling circuit as a linear function of V and I_{sq} ; i.e., we can obtain the rf fields in the coupling circuit using only the parameters of the SQUID.

Finally, the impedance Z_{AB} seen by the SQUID washer is derived as follows. From Fig. 1, an expression for the voltage V can be written as

$$V = j\omega L_s \left(I_{sq} + \sum_{m=1}^N I_m \right) + j\omega \Delta L_{sl} \left[(N+1) I_{sq} + \sum_{m=1}^N (N+1-m) I_m \right], \quad (6)$$

where $L_s = 1.25\mu_0 a$ is the inductance of the SQUID washer due to the square hole.¹² Here, a is the side length of the hole. The first term in Eq. (6) represents the voltage drop due to the hole inductance L_s ; note that the current flowing along the hole of the SQUID washer is given by the summation of I_{sq} and I_m , as shown in Fig. 1. The second term in Eq. (6) represents the voltage drop caused by the slit inductance L_{sl} of the SQUID washer.

Substituting the expression for I_m given in Eq. (4) into Eq. (6), we obtain a linear relation between the voltage V and the current I_{sq} . This linear relation gives implicitly the impedance Z_{AB} ,

$$Z_{AB} = V/I_{sq} \quad (7)$$

III. NUMERICAL RESULTS

In Fig. 3(a), an example of the rf properties of the coupling circuit calculated using the present model is shown. The absolute value of the impedance Z_{AB} seen by the SQUID washer is calculated as a function of frequency; the frequency region is $f = 0.1$ –200 GHz. The parameters of the SQUID are: the hole side length $a = 100 \mu\text{m}$; the number of turns of the input coil $N = 55$; the width w and

the spacing s of the input coil $w = s = 2 \mu\text{m}$; the thickness of the insulator $d = 1 \mu\text{m}$; and the dielectric constant of the insulator $\epsilon_r = 2.2$. The quality factor of the transmission line is chosen as $Q = 50$. From these parameters, we obtain the inductances $L_s = 157 \text{ pH}$ and $L_{s1} = 16 \text{ pH}$. The terminals of the input coil are open, and no damping resistors are used.

As shown in Fig. 3(a), there are many resonant structures in the $Z_{AB}-f$ characteristic. The characteristic is very different from the case of the isolated SQUID, where the impedance is given simply by $Z_{AB} = j\omega(L_s + L_{s1})$. It has been shown that these resonant structures arise from the standing wave occurring between the input coil and the SQUID washer.^{4,9} corresponding to the half-wavelength resonance of the transmission line in this case.

It can be shown that there are two types of standing waves. In the low-frequency region, the input coil acts as a stripline with the SQUID washer as the ground plane. In this case the frequencies causing the standing wave are determined by the total length of the input coil; hereafter, we call this resonance the input coil resonance. The resonant structures below $f = 30 \text{ GHz}$ shown in Fig. 3(a) correspond to the input coil resonance. In this region, the input coil resonance affects significantly the $Z_{AB}-f$ relation. The effect, however, becomes smaller when the frequency becomes larger, as shown in Fig. 3(a). When the frequency becomes much higher, another type of standing wave occurs between the input coil and the SQUID washer. In this case, the SQUID washer acts as a stripline with the input coil as the ground plane, in contrast to the case of the input coil resonance. Therefore, in this case, the frequencies for the standing wave are determined by the length of the SQUID washer; hereafter, we call this resonance the washer resonance. The resonant structures above $f = 70 \text{ GHz}$ shown in Fig. 3(a) correspond to the washer resonance.

The properties of the input coil resonance shown in Fig. 3(a) change considerably with the boundary condition of the input coil. As an example, we show in Fig. 3(b) the $Z_{AB}-f$ relation for the case when one terminal of the input coil is shorted to the SQUID washer;⁶ the terminals D and D' shown in Fig. 2 are shorted, while the terminals C and C' are open. As shown in Fig. 3(b), Z_{AB} has peak values at different frequencies, corresponding to the quarter-wavelength resonance of the transmission line. Furthermore, the resonant structures in Z_{AB} are smaller than the case shown in Fig. 3(a). The different results in Figs. 3(a) and 3(b) show the importance of the boundary condition to the property of the input coil resonance. With respect to the suppression of the input coil resonance, the impedance shown in Fig. 3(b) is better than that in Fig. 3(a). Therefore, this method of shorting one terminal of the input coil to the SQUID washer is useful not only for simplifying the fabrication process, but also for suppressing the input coil resonance.

The input coil resonance can also be suppressed using damping resistors. In Fig. 3(c), the effect of a damping resistor on the impedance Z_{AB} is shown. One terminal of the input coil is shorted to the SQUID washer as in the

case of Fig. 3(b), and the other terminal of the input coil (terminal C in Fig. 2) is connected to the SQUID washer (terminal C' in Fig. 2) through a series R_x-C_x shunt.⁸ The values are $R_x = z_0 = 143 \Omega$ and $C_x = 160 \text{ pF}$, where z_0 is the characteristic impedance of the transmission line. As shown, the input coil resonances are completely suppressed by the damping resistor R_x . It can be shown that the value of R_x is not sensitive, i.e., values of R_x much larger than z_0 also suppress the input coil resonances.

The resistance R_x , however, cannot suppress the washer resonances, as shown in Fig. 3(c). Since the input coil acts as the ground plane for this resonance, it is reasonable that the resistance R_x is not useful in suppressing this feature. In the design of this device,⁶ the SQUID geometry was chosen so that the washer resonances are much higher than the typical operating frequency of the Josephson junctions in order to avoid the effects of the washer resonances.

The resonant structure in Z_{AB} can also be suppressed using a damping resistor.^{5,13} R_d connected in parallel with the SQUID washer. In Fig. 3(d) we show the impedance Z_{AB} when a damping resistance $R_d = 3 \Omega$ is connected between terminals A and B shown in Fig. 1; the boundary conditions for the input coil are the same as those for the case shown in Fig. 3(b). As shown, both the input coil resonances and the washer resonances are suppressed by the damping resistor R_d . In particular, the washer resonances are well suppressed. On the other hand, the suppression of the input coil resonances is not as good as that obtained using an R_x-C_x shunt: The first large peak in the $Z_{AB}-f$ response is well suppressed, but higher-frequency structures are not suppressed. It can be shown, however, that the suppression of the input coil resonances improves if a damping resistor with smaller value is used, such as $R_d = 1 \Omega$. It can also be shown that the value of R_d necessary to suppress the resonant structure depends both on the number of turns in the input coil N and the slit inductance L_{s1} of the SQUID washer: R_d decreases with increasing N and decreasing L_{s1} . It must be mentioned that the resonant structures in Z_{AB} can be almost completely suppressed by using both the R_x-C_x shunt and R_d , as can be seen from the results shown in Figs. 3(c) and 3(d).

IV. ANALYTICAL RESULTS

It will be useful to derive a simple analytical expression for the impedance Z_{AB} in order to study the properties of Z_{AB} . In the following, we treat the case shown in Fig. 3(a), i.e., the input coil is open and no damping resistors are used. This configuration is used in conventional designs. We also consider the input coil resonance, which is important for the usual operation of the SQUID.

In order to obtain an analytical expression for Z_{AB} , we assume the simple case where the slit inductance of the SQUID washer L_{s1} can be neglected. We also consider only the low-frequency region where the washer resonance can be neglected. In this case, we can obtain an analytical expression for the impedance Z_{AB} as (see Appendix C)

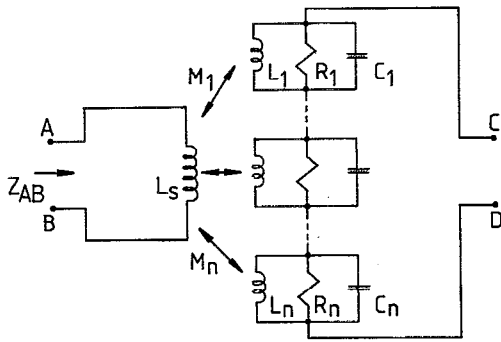


FIG. 4. The equivalent circuit of the SQUID coupled to the input coil for the conventional case shown in Fig. 3(a); both terminals of the input coil are open and no damping resistors are used. The input coil is represented by a set of resonant circuits, each of which couples to the SQUID via a mutual inductance $M_n = \alpha_n(L_s L_n)^{1/2}$, where α_n is the coupling constant.

$$Z_{AB} = j\omega L_s \left(1 - \alpha_1^2 + \alpha_1^2 (1 - \alpha_1^2) \right) \times \frac{(2/kl_t) \tan(kl_t/2)}{1 - (2\alpha_1^2/kl_t) \tan(kl_t/2)}, \quad (8)$$

where $\alpha_1 = NL_s/[L_s(N^2L_s + L_{st})]^{1/2}$ is the coupling constant between the SQUID coil and the input coil for dc magnetic fields.^{9,10} The term NL_s in α_1 is the mutual inductance, and the term $N^2L_s + L_{st}$ is the inductance of the input coil for dc fields. The term $L_{st} = (d\mu_0/w)l_t$ is the stripline inductance of the input coil, and l_t is the total length of the input coil.

From Eq. (8) we can discuss the properties of Z_{AB} . In the previous papers,^{9,10} the circuit model shown in Fig. 4 was proposed for a SQUID coupled to an input coil. In that model, the input coil is represented by a set of resonant circuits, each of which corresponds to the standing wave in the input coil resonance. The SQUID coil couples to each resonant circuit through a mutual inductance $M_n = \alpha_n(L_s L_n)^{1/2}$, where α_n is the coupling constant.

In the circuit model shown in Fig. 4, the values of C_n , L_n and R_n have been obtained from the parameters of the SQUID as^{9,10}

$$C_n = C_0 l_t / 8, \quad L_n = 8L_0 l_t / \pi^2 (2n - 1)^2, \quad (9)$$

$$R_n = Q_n (L_n / C_n)^{1/2},$$

where $C_0 = \epsilon_0 \epsilon_r / d$ and $L_0 = d\mu_0 / w$ are the capacitance and the inductance of the transmission line per unit length, respectively, and l_t is the total length of the input coil. Note that in Eq. (9) the term $1.25\mu_0 a N^2$ must be added⁹ to the inductance L_1 for the case $n = 1$.

The values of the coupling constant α_n , however, were not determined in the previous papers. Using Eq. (8), we can obtain an expression for α_n as follows. It can be seen from Eq. (8) that the impedance Z_{AB} has peak values whenever

$$\tan(kl_t/2) = kl_t/2\alpha_1^2. \quad (10)$$

The above equation gives implicitly the resonant frequencies f_n in the $Z_{AB}-f$ relation. It can be shown that the

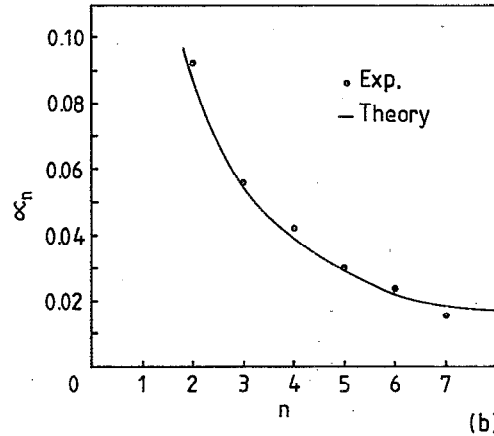
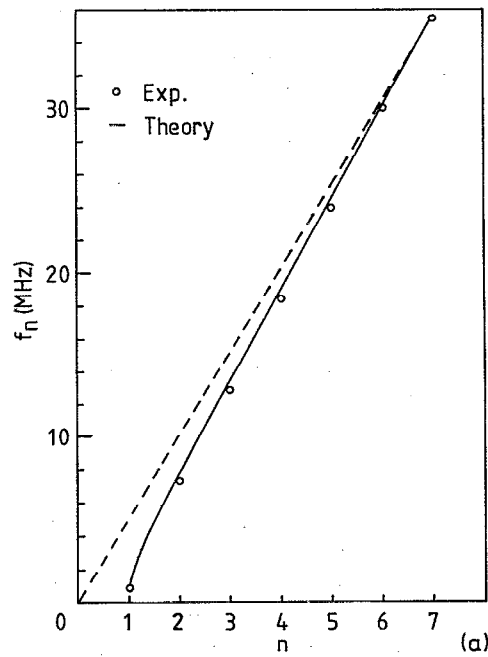


FIG. 5. (a) The resonant frequencies f_n and (b) the coupling constants α_n of the equivalent circuit shown in Fig. 4. The solid lines are the theoretical results calculated from Eqs. (10) and (11), and the circles are experimental results reported in Ref. 10. In the calculation of α_n , we use the theoretical value $\alpha_1 = 0.95$ calculated from the relation $\alpha_1 = NL_s/[L_s(N^2L_s + L_{st})]^{1/2}$, while the experimental value of α_1 was $\alpha_1 = 0.93$.

resonant frequencies are given roughly by $f_n = (2n - 1) \times (v_c/2l_t)$, where n is an integer and the number $2n - 1$ corresponds to the number of the standing wave. Expanding Eq. (8) around the resonant frequencies and comparing with the expression for Z_{AB} obtained from Fig. 4 [Eq. (8) in Ref. 9], we obtain expressions for C_n , L_n , R_n and α_n shown in Fig. 4. The expressions for C_n , L_n and R_n are the same as those given in Eq. (9), and the coupling constant α_n is given by

$$\alpha_n^2 = \alpha_1^2 (1 - \alpha_1^2) \frac{8}{\pi^2} \frac{1}{(2n - 1)^2}, \quad (11)$$

for $n \geq 2$.

In Fig. 5(a), the solid line shows the dependence of the resonant frequency f_n on the number of the standing wave

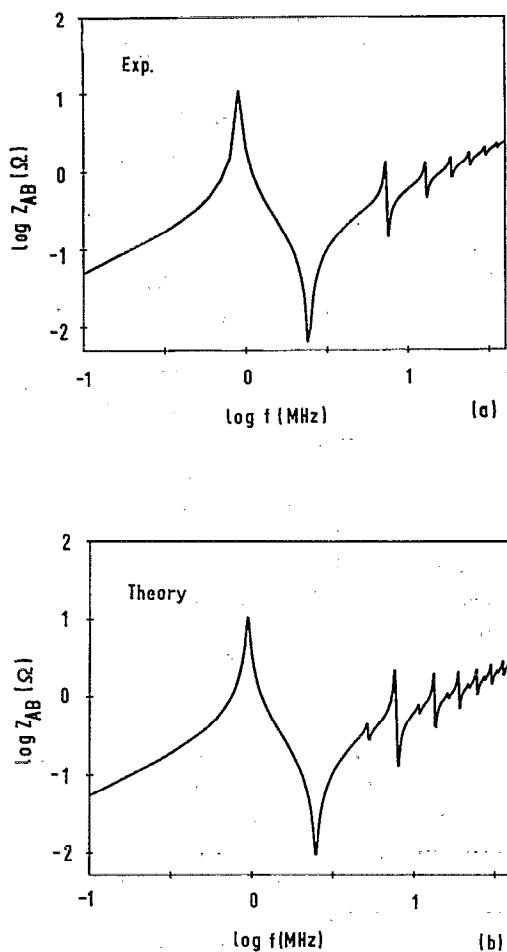


FIG. 6. Comparison between theory and experiment of Z_{AB} in the case of the input coil resonance. (a) Experimental result reported in Ref. 10, which was measured using an expanded model with an expansion factor $F = 500$; (b) Theoretical result calculated from the present model. Note that no adjustable parameters are used in the calculation. The frequency range $f = 0.1$ – 40 MHz used in the expanded model corresponds to $f = 50$ – 20 GHz in the practical SQUID.

n , which is calculated from Eq. (10). In the calculation, we use the same SQUID parameters as those for the case shown in Fig. 6. As can be seen in Fig. 5(a), when the value of n becomes large, the value of f_n approaches the frequency $f_n = (2n - 1)(v_c/2l_t)$ corresponding to the half-wavelength resonance of the transmission line, which is shown by a dashed line in Fig. 5(a). For the case of small n , however, the deviation between the two curves becomes large, especially for the case $n = 1$. This difference is caused by the existence of the slit in the SQUID washer.

In Fig. 5(b), the solid line shows the dependence of the coupling constant α_n on n , which is calculated from Eq. (11). As shown in Fig. 5(b), the value of α_n decreases approximately inversely with n . This result must be emphasized, since this result means that the effect of the input coil resonance on the impedance Z_{AB} becomes smaller as the number n (or the frequency) increases. This property of Z_{AB} has also been shown numerically in Fig. 3(a).

V. COMPARISON WITH EXPERIMENT

In order to verify the validity of the present circuit model, we have compared the rf properties calculated from

the model with experimental results. First, we consider the impedance in the frequency region of the input coil resonance. In this frequency region, the impedance Z_{AB} can be measured using an expanded model of the circuit.^{9,10}

In Fig. 6, the calculated rf properties are compared with the experimental result: Fig. 6(a) shows the experimental results reported in Ref. 10, and Fig. 6(b) shows the calculated result. The former were obtained from measurement on an expanded model (expansion factor $F = 500$) with Cu electrodes. The SQUID model parameters were $a = 5$ cm, $w = s = 1$ mm, and $d = 0.5$ mm, which are 500 times larger than the parameters used in obtaining Fig. 3(a), while the parameters $N = 55$ and $\epsilon_r = 2.2$ are the same as for the case shown in Fig. 3(a). The boundary conditions for the input coil are also the same as for the case shown in Fig. 3(a); two terminals of the input coil are open, and no damping resistors are used. The quality factor Q of the transmission line is calculated by the loss of the Cu electrodes by using the expression $Q = (2\sigma\mu_0 d^2 \omega)^{1/2}$, where $\sigma = 5 \times 10^7$ S/m is the conductivity of Cu. The frequency range $f = 0.1$ – 40 MHz shown in Fig. 6 corresponds to $f = 50$ MHz– 20 GHz in the practical case.

As shown in Fig. 6, the present model explains well the experimental results. The Z_{AB} – f characteristic calculated from the present model agrees quantitatively with the observed resonant structures in Z_{AB} ; if we take into account the losses in the insulator, the agreement between the two curves will become much better with respect to the peak values of Z_{AB} . It must be noted that the present model uses only the parameters of the SQUID: No adjustable parameters are used in the calculation. This good agreement confirms the validity of the present model.

In Fig. 5, we also compare the analytical results on the resonant frequencies f_n and the coupling constants α_n with the experimental results. The solid lines in Figs. 5(a) and 5(b) are calculated from Eqs. (10) and (11), respectively. In the calculation of Eq. (11), we use $\alpha_1 = 0.95$, which is calculated from the relation $\alpha_1 = NL_s/[L_s(N^2L_s + L_{st})]^{1/2}$. The circles in the figure are experimental results reported in Ref. 10. As shown in Fig. 5, good agreement is also obtained in this case.

It must also be mentioned that the present model can explain well the effect of the damping resistors on the impedance Z_{AB} . It can be shown that the experimental results^{9,10} on the suppression of the input coil resonances by the use of damping resistors are explained quantitatively with the present model.

Next, we consider the case of the washer resonance. In this case, it is very difficult to measure the rf properties of the SQUID, even with the expanded model, due to the very high operating frequency. Therefore, it is difficult to compare the rf properties calculated from the present model directly with experiment. It is expected, however, that the resonant structures in Z_{AB} cause the so-called resonant current steps in the current-voltage (I – V) characteristics of the SQUID. Therefore, we compare the resonant frequencies in Z_{AB} with the experimental voltages corresponding to the resonant current-steps.

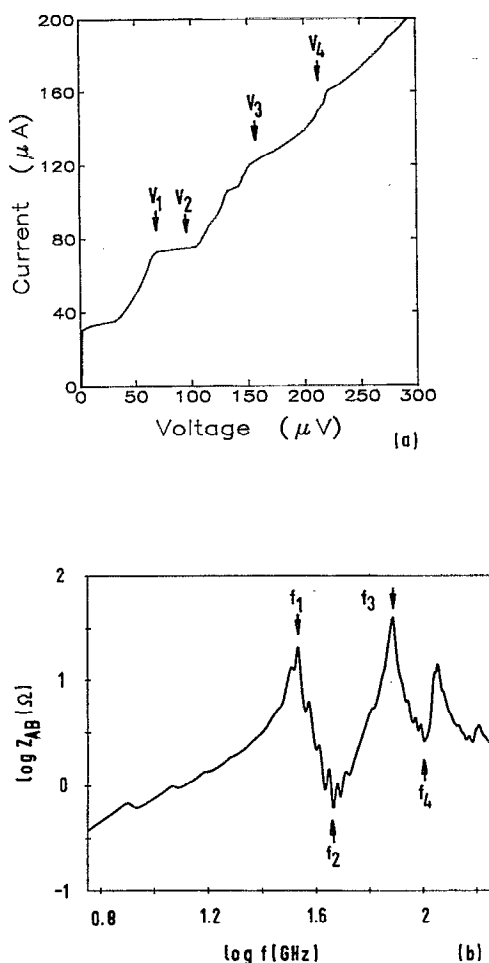


FIG. 7. (a) Current-voltage characteristics of a SQUID with an integrated input coil. (b) $Z_{AB} - f$ characteristics of the SQUID calculated from the present model. The resonant frequencies corresponding to the washer resonances are denoted by f_n : $f_1 = 34$ GHz, $f_2 = 46$ GHz, $f_3 = 77$ GHz, and $f_4 = 101$ GHz. The voltages obtained from the Josephson relation $V_n = f_n \Phi_0$ are shown by arrows.

In Fig. 7(a), the I - V characteristic of a SQUID¹⁴ coupled to a multiturn input coil is shown. The parameters of the SQUID are: $N = 12$, $a = 18$ μm , $L_s = 28.3$ pH, $L_{s1} = 22.5$ pH, and $s = w = 3$ μm . For this device, Nb_2O_5 ($d = 0.075$ μm and $\epsilon_r = 29$) was used as the insulator between the SQUID coil and the input coil in order to emphasize the effect of the input coil: The effect of the input coil is usually much weaker than the present case, since an insulator with smaller ϵ_r is normally used. An R_x - C_x shunt with $R_x = 8.5$ Ω and $C_x = 193$ pF is used to suppress the input coil resonance, as shown in Fig. 3(c).

In Fig. 7(b), the impedance Z_{AB} calculated from the parameters of the SQUID is shown. A quality factor $Q = 30$ has been chosen. In the calculation of Z_{AB} , it must be noted that for a practical SQUID, a capacitance C_j exists across the Josephson junction. The capacitance C_j is expected to affect the I - V curve of the SQUID at high voltages (or at high frequencies, as for the washer resonance). It has been shown^{13,15} that the effect of C_j can be approximately taken into account by connecting the capacitance

$C_j/2$ in parallel with the SQUID washer; i.e., between terminals A and B of the SQUID washer shown in Fig. 1. The factor $\frac{1}{2}$ is due to the series connection of the two junction capacitances. In the present experiment, the value $C_j = 1$ pF is estimated from the size of the Josephson junction. In Fig. 7(b), therefore, the impedance Z_{AB} is shown for the case where $C_j/2 = 0.5$ pF is connected between terminals A and B of the SQUID washer.

As shown in Fig. 7(b), the input coil resonances are suppressed well by the R_x - C_x shunt. The washer resonance, however, cannot be suppressed by the R_x - C_x shunt as discussed in Fig. 3(c). In Fig. 7(b), the frequencies corresponding to the washer resonances are denoted by f_n . The voltages obtained from the Josephson relation $V_n = f_n \Phi_0$, where Φ_0 is the flux quantum, are shown by arrows in Fig. 7(a). The theoretical values are $V_1 = 69$ μV , $V_2 = 95$ μV , $V_3 = 159$ μV , and $V_4 = 210$ μV . For reference, the voltages are $V'_1 = 71$ μV , $V'_2 = 95$ μV , $V'_3 = 180$ μV , and $V'_4 = 221$ μV in the case $C_j = 0$.

As shown in Fig. 7(a), the voltages predicted from the present model explain the experimental voltages corresponding to the resonant current steps. The experimental voltages $V = 69$, 152 , and 225 μV agree well with the theoretical values $V_1 = 69$ μV , $V_3 = 159$ μV and $V_4 = 210$ μV , respectively. For a different sample, the resonant current steps are observed at the voltages $V = 102$ and 216 μV . These experimental voltages agree with the theoretical values $V_2 = 95$ μV and $V_4 = 210$ μV . Experimentally, resonant current steps which one observed may depend on the parameters of the Josephson junctions, i.e., the junction critical current and junction shunt resistance. At present, however, the current step observed at $V = 132$ μV shown in Fig. 7(a) cannot be explained by the resonant structure in Z_{AB} . Other parasitic elements existing around the Josephson junctions, which are not taken into account in the present model, may cause this resonant step. Nonlinear dynamics of the SQUID may also explain the current step at $V = 132$ μV ; for example, if we assume a subharmonic resonance, we can expect a current step at $V = 2 V_1 = 138$ μV .

As mentioned above, the present circuit model quantitatively explains the experimental results without any adjustable parameters. The good agreement in each case confirms the validity of the present model.

VI. CONCLUSION

We have developed a complete circuit model of a SQUID coupled to the multiturn input coil. Using this model, we can calculate the rf properties of the coupled SQUID from the parameters of the SQUID. The rf properties calculated using the present model explain well the experimental results. The properties of the input coil resonances and the washer resonances can be quantitatively explained without any adjustable parameters. Therefore, we can use the present model to study the effect of the input coil on SQUID characteristics. The present model is also useful for the design of highly sensitive SQUIDs.

ACKNOWLEDGMENTS

The authors acknowledge gratefully Dr. S. Kohjiro (ETL in Japan) for his helpful discussions. K. E. also acknowledges support from Kyushu University of Japan.

APPENDIX A: COEFFICIENTS $A_m - H_m$ IN EQS. (4) AND (5)

Substituting Eqs. (4) and (5) into Eqs. (1) and (2), we can obtain the relation among the coefficients $A_m - H_m$ as

$$A_{m+1} = A_m \cos kl_m - jE_m \sin kl_m - j(m-1)X_{s1} \sin kl_m - jX_{s1} \left(\sum_{i=2}^{m-1} (m-i)A_i \right) \sin kl_m \quad (A1)$$

$$B_{m+1} = B_m \cos kl_m - jF_m \sin kl_m - jX_{s1} \left(\sum_{i=2}^{m-1} (m-i)B_i \right) \sin kl_m \quad (A2)$$

$$C_{m+1} = C_m \cos kl_m - jG_m \sin kl_m + j \sin kl_m - jX_{s1} \left(\sum_{i=2}^{m-1} (m-i)C_i \right) \sin kl_m \quad (A3)$$

$$D_{m+1} = D_m \cos kl_m - jH_m \sin kl_m - jmX_{s1} \sin kl_m - jX_{s1} \left(\sum_{i=2}^{m-1} (m-i)D_i \right) \sin kl_m \quad (A4)$$

$$E_{m+1} = -jA_m \sin kl_m + E_m \cos kl_m + (m-1)X_{s1} \cos kl_m + X_{s1} \left(\sum_{i=2}^{m-1} (m-i)A_i \right) \cos kl_m \quad (A5)$$

$$F_{m+1} = -jB_m \sin kl_m + F_m \cos kl_m + X_{s1} \left(\sum_{i=2}^{m-1} (m-i)B_i \right) \cos kl_m \quad (A6)$$

$$G_{m+1} = -jC_m \sin kl_m + G_m \cos kl_m - \cos kl_m + X_{s1} \left(\sum_{i=2}^{m-1} (m-i)C_i \right) \cos kl_m \quad (A7)$$

$$H_{m+1} = -jD_m \sin kl_m + H_m \cos kl_m + mX_{s1} \cos kl_m + X_{s1} \left(\sum_{i=2}^{m-1} (m-i)D_i \right) \cos kl_m \quad (A8)$$

for $m \geq 2$, where $X_{s1} = j\omega\Delta L_{s1}/z_0$ is the parameter representing the effect of the slit inductance of the SQUID, L_{s1} . Note that the summations on the right-hand side of Eqs. (A1)–(A8) are set to zero for the case $m = 2$.

As shown above, Eqs. (A1)–(A8) give the iterative relations for the values of $A_m - H_m$. The initial values $A_2 - H_2$ can be obtained from Eqs. (1)–(5) as $A_2 = \cos kl_1$, $B_2 = -j \sin kl_1$, $C_2 = D_2 = 0$, $E_2 = -j \sin kl_1$, $F_2 = \cos kl_1$, and $G_2 = H_2 = 0$, where l_1 is the length of the first section of the input coil. Therefore, using these initial values and Eqs. (A1)–(A8), we can

calculate iteratively the values of $A_m - H_m$ when the parameters of the SQUID, i.e., the parameters k , l_m , and X_{s1} , are known.

APPENDIX B: BOUNDARY CONDITIONS OF THE INPUT COIL

The boundary conditions of the input coil determine the values of I_1 and $V_{tb,1}$ in Eqs. (4) and (5) as follows. As can be seen from Fig. 2, the boundary conditions of the input coil give the relation among I_1 , $V_{tb,1}$, I_{N+1} , and $V_{ta,N+1}$, which are the rf currents and the voltages at the ends of the input coil, as shown in Fig. 2 (terminals C and D).

First, we consider the case where the terminals of the input coil are open, which is used in obtaining Fig. 3(a). In this case, the boundary conditions are given by

$$I_1 = I_{N+1} = 0. \quad (B1)$$

Next, we consider the case used in obtaining Fig. 3(c). In this case, the terminal D of the input coil shown in Fig. 2 is shorted to the terminal D', and a series $R_x - C_x$ shunt is connected between terminals C and C', as shown in Fig. 2. Therefore, the boundary conditions are given by

$$V_{ta,N+1} = 0, \quad (B2)$$

$$V_{tb,1} = (R_x + 1/j\omega C_x)(-I_1). \quad (B3)$$

It must be mentioned that, in this case, the current I_1 flows into the SQUID washer through the $R_x - C_x$ shunt and cancels the image current $-I_1$. In this case, therefore, the summation of I_i and I_m given in Eqs. (3) and (6) must start from $i = 2$ and $m = 2$, respectively. Furthermore, the third terms in the right-hand side of Eqs. (A1) and (A5) must be deleted in this case.

Finally, we consider the case where the resistance is attached between the two terminals of the input coil; the resistance R_i is connected³ between the terminals C and D shown in Fig. 2. In this case, the boundary conditions are given by

$$I_1 = I_{N+1}, \quad (B4)$$

$$V_{ta,N+1} = V_{tb,1} + I_1 R_i + V_{sb,1} - V_{sa,N+1}. \quad (B5)$$

Substituting the expressions for I_{N+1} and $V_{ta,N+1}$ given in Eqs. (4) and (5) into the boundary conditions given above, we can obtain the variables I_1 and $V_{tb,1}$ as a linear function of V and I_{sq} . Therefore, substituting these results into Eqs. (4) and (5), we can calculate the rf current I_m and voltage $V_{ta,m}$ in each section of the coupling circuit as a linear function of V and I_{sq} , i.e., we can obtain the rf fields in the coupling circuit.

APPENDIX C: DERIVATION OF EQ. (8)

The analytical expression of Z_{AB} given in Eq. (8) can be obtained as follows. If we consider the case where the value of the slit inductance L_{s1} is negligibly small compared with the hole inductance L_s , we can obtain from Eqs. (1)–(5) a simple expression for Z_{AB} as

$$\frac{1}{Z_{AB}} = \frac{1}{j\omega L_s} + (j/z_0 \sin kl_i) \left[\sum_{p=2}^N \sin \left(k \sum_{i=p}^N l_i \right) \right] \\ \times \left[\sum_{m=2}^N \sin \left(k \sum_{i=1}^{m-1} l_i \right) \right] \\ - \left(\frac{j}{z_0} \right) \sum_{m=3}^N \sum_{p=2}^{m-1} \sin \left(k \sum_{i=p}^{m-1} l_i \right). \quad (C1)$$

Since we are considering the input coil resonance, the values of the kl_i in Eq. (C1) are much smaller than unity, where l_i is the length of each section. In this case, we can approximate the summation in Eq. (C1) by an integral. Furthermore, an analytical solution of the integral can be obtained by approximating the length l_i in Eq. (C1) by the averaged value, i.e., $l_i = \langle l \rangle = l_t/N$, where l_t is the total length of the input coil. Substituting the analytical solution of the integral into Eq. (C1), we obtain the analytical expression for Z_{AB} as given in Eq. (8).

¹V. J. de Waal, T. M. Klapwijk, and P. van den Hamer, J. Low Temp. Phys. **53**, 287 (1983).

- ²C. Hilbert and J. Clarke, J. Low Temp. Phys. **61**, 237 (1985).
³J. Knuutila, A. Ahonen, and C. Tesche, J. Low Temp. Phys. **68**, 269 (1987).
⁴T. Ryhänen, H. Seppä, R. Ilmoniemi, and J. Knuutila, J. Low Temp. Phys. **76**, 287 (1989).
⁵V. Foglietti, W. J. Gallagher, M. B. Ketchen, A. W. Kleinsasser, R. H. Koch, and R. L. Standstrom, Appl. Phys. Lett. **55**, 1451 (1989).
⁶R. Cantor, T. Ryhänen, D. Drung, H. Koch, and H. Seppä, IEEE Trans. Magn. **MAG-27**, 2927 (1991).
⁷V. Foglietti, M. E. Giannini, and G. Petrocco, IEEE Trans. Magn. **MAG-27**, 2989 (1991).
⁸H. Seppä and T. Ryhänen, IEEE Trans. Magn. **MAG-23**, 1083 (1987).
⁹K. Enpuku and K. Yoshida, J. Appl. Phys. **69**, 7295 (1991) (Part I).
¹⁰K. Enpuku, T. Tanaka, and K. Yoshida, IEICE Trans. E **74**, 2020 (1991).
¹¹S. Kohjiro (private communication).
¹²J. M. Jaycox and M. B. Ketchen, IEEE Trans. Magn. **MAG-17**, 400 (1981).
¹³K. Enpuku, K. Sueoka, K. Yoshida, and F. Irie, J. Appl. Phys. **57**, 1691 (1985).
¹⁴R. Cantor, T. Ryhänen, and H. Seppä, in *Superconducting Devices and their Applications, Springer Proceedings in Physics*, edited by H. Koch and H. Lubbig (Springer, Berlin, in press).
¹⁵H. H. Zappe and B. S. Landman, J. Appl. Phys. **49**, 4149 (1978).